7

Novel Synthesis for Functional Polymers and Nanomaterials: Electrochemical Synthesis; Molecular Imprinting Synthesis; Molecular-Level Hybridization

Kyung Moon Choi

University of California, Irvine, Chemistry 5003 Reines Hall, Irvine, CA 92697, USA

Outline

Introduction

In the past, synthetic materials have been used mostly for bio or chemical applications, chemists and materials scientists are looking to the applications of nanotechnology in physics and engineering to improve the performance of aerospace and optoelectronic devices.
In particular, novel synthesis of functional nanomaterials has taken great attention to the fabrication of integrated aerospace and optoelectronic devices on small chips due to the special advantages that arise from small sizes, such as "quantum size effects." [1-10] The overall object of nanomaterial synthesis is for small-scale chemical reactions on a small chip.
However, conventional synthesis has shown limitations in producing advanced nanomaterials that create our desired properties; in order to overcome the limitations, chemists have taken efforts to discover new synthetic approaches that create desired properties at the nanoscales.
New synthesis often requires an important aspect of "combinatorial knowledge"; which means physicists, chemists, materials scientists, and engineers are working together to molecularly design new molecular structures and create desired properties that fit them into their optoelectronic devices. The category of "combinatorial synthetic technology" includes collaborative works carried out by scientists in diverse fields, physicists, chemists, materials scientists, and engineers.
The author of this chapter has a multidisciplinary background in applied physics, synthetic chemistry, materials science, and nanotechnology to create desired properties in advanced functional materials for optoelectronic applications based on combinational knowledge. **[11-30]** The author's intentions and directions toward unconventional synthesis for optoelectronic applications often lead to breakthroughs in chemistry and materials science.
In this chapter, novel synthetic routes are introduced to create specific and desired properties in advanced functional materials; 1) Electrochemical synthesis produces "conducting polymers" to fabricate flexible electronic devices. 2) Molecular imprinting synthesis was demonstrated to synthesize a sensing polymer with molecular recognition sites that can detect "specific target molecules" for biochemical sensor applications. 3) Molecular-level hybridization was introduced to produce "molecular-level composites" by mixing multiple components at the nanoscales without phase separation.

A Brief Description of Novel Syntheses

The 1st part introduces "electrochemical synthesis" that produces "conducting polymers" prepared using cyclic voltammetry. Conductive polymers such as doped polyaniline or polyindole can be used to fabricate portable electronics due to their lightweight advantage.
The 2nd part, "molecular imprinting synthesis" was demonstrated to create "molecular recognition sites." These recognition sites (receptors or binding sites) can be molecularly designed and synthesized by "molecular imprinting synthesis," particularly for use in biochemical sensors or detection devices. The molecular recognition will take place by the extraction/rebinding process of templates to detect specific target molecules.
In the 3rd part, "molecular-level hybridization" was introduced that mixes up multiple components at the nano-scales to produce "molecular-level hybrid composites."
Hybrid composites prepared by the molecular-level hybridization showed relatively less phase separation due to the homogeneity at the molecular level. These composites are mixed at the nanoscales and so often resulted in the creation of NEW properties/functionalities that the individual component doesn't have.

As our demand for miniaturization increases, the demand for smaller and more compact electronic devices has received a lot of attention. This chapter will introduce novel synthetic approaches that produce advanced functional materials based on extensive knowledge in nanotechnology.
So, this chapter will be intended for a wide range of readers worldwide such as physicists, chemists, engineers, materials scientists, and biologists.

Electrochemical Synthesis

Prior to the technological revolution, natural materials have been used in our daily lives, but natural materials have a lot of limitations. As our needs for advanced materials increased, synthetic materials, especially functional polymers have been used to meet our specific demands.
However, synthetic materials also have limitations. Synthetic materials are mostly materials designed to meet our requirements, for example, portable and flexible electronics required lightweight, highly conductive materials, and specific requirements led to the discovery of conductive polymers.
Usually, conductive polymers are prepared by simply injecting a conductive filler into a polymer host, but phase separation often occurs.
To solve a phase separation, chemists designed novel molecular structures, “conjugated double bonds” that can produce conductive polymers by doping with donors or acceptors through electrochemical or chemical oxidations.
Aromatic compound-based conducting polymers have been prepared by electrooxidation; polypyrrole **[31, 32]**, polyaniline **[33],** polyazulene **[34],** polycarbazole **[35],** and polythiophene **[36].** Bargons et. al. reported that polyazulene, polythiophene, polycarbazole, polypyrene, and poly-triphenylene have been obtained from electrochemical polymerization. **[37]**
In order to obtain conductive polymers as forms of anodic precipitates, we considered the following electrochemical conditions in our earlier study. **[15]**
First, conductive polymers were prepared on the anode from aromatic monomers with anodic peak potentials of below 2V. With potentials above 2V, the possibility of oxidation of solvents and of supporting electrolytes increases with the increase in anodic potential.
Second, we considered the stability of radical cations formed around the anode. The anodic products are obtained from the electropolymerization of radical cations formed around the anode as precipitates. Therefore, radical cations must not be diffused to the bulk solution until they are polymerized.
The proper stability of radical cations is related to the solvent effect. That is, in order to obtain the products in the form of precipitates, the selection of proper solvents is also important.
Accordingly, the determination of proper solvents and of electrochemical conditions for various aromatic compounds have been carefully studied.
Third, the suitable electrode composition was also essential. In principle, a three-electrode cell system was adopted for obtaining conducting polymers in an electrooxidation system. The physical properties of polymers prepared from the three-electrode system are better than those of polymers obtained from the two-cell system.
In short, conducting polymers were synthesized from aromatic monomers with anodic peak potentials of below 2 V due to the stability of radical cations formed around the anode. These anodic precipitates were prepared by the electropolymerization of radical cations formed around the anodic electrode. So, the selection of a proper solvent and electrochemical conditions are critical for aromatic compounds to keep the stability of radical cations around the electrode.

In our earlier study, polyindole doped with tetrafluoroborate [(PI)BF_4] was produced via electrochemical reactions and we elucidated on the morphology, thermal stability, magnetic property, and the electrical conduction mechanism. **[15]**
We compared it to other studies; Tourillon et. al. synthesized polyindole films, but it was very brittle and cracked easily when removed from the anode. **[38]**
We focused on the preparation of polyindol conducting polymer with good mechanical quality by controlling the most suitable solvent and electrochemical conditions; in our study, polyindole tetrafluoroborate, (PI)BF_4, was produced as an anodic precipitate with good mechanical property from a 0.2M indole monomer in an [acetonitrile/benzonitrile/water] solution containing 0.1M tetraethylammonium tetrafluoroborate, (TEA)BF_4 by supplying a potential of 0.7V.
We also obtained (PI)BF_4 polymers as a powder form from the electrooxidation reactions; because, film-type samples in the earlier study have shown disadvantages for mass production, reproducibility, handling, and shaping which polymer samples in powder form can overcome.
In cyclic voltammetry experiments, the electrode reaction in an indole solution was reversible and the number of related electrons was 2. Our experiments suggested that the electropolymerization of polyindole proceeded by the formation of radical cations as intermediates.

Sample Preparations

Polyindole tetrafluoroborate [(PI)BF_4] was electrochemically synthesized from a 0.2M indole monomer in an [acetonitrile/benzonitrile/water] solution containing 0.1 M tetraethylammonium tetrafluoroborate, (TEA)BF_4, as a supporting electrolyte.
The three-electrode cell composition was equipped with Pt plates as a working electrode/counter electrode shaped like a sheet, and an Ag/AgCl electrode as a reference electrode.
The temperature of the solution in the reaction cell was also maintained at 25°C, using a circulator (Lauda Co.). A nitrogen stream was passed through the monomer solution for 30 min before each measurement in order to remove the dissolved oxygen.
(PI)BF_4 polymer was obtained as insoluble precipitates on the anode by applying using a potential of 0.7V. With a supplied external potential of 0.7V, the color of the solution around the anode changed from dark green to maroon black.
As oxidation progressed, the solution in contact with the anode was extracted, and the UV measurement for this extracted solution was performed.
The anodic precipitates were then removed from the electrode, rinsed with acetonitrile, and dried in a vacuum oven for 2 days until a constant weight was achieved. The (PI)BF_4 polymer was a black conducting powder, which in its oxidized state was stable in air.

Conductivity Measurements

(PI)BF_4 polymers were prepared from the electropolymerization by supplying a potential of 0.7 V during a synthesis time of 10 h. The resultant anodic precipitates were dried in a vacuum oven. Finally, the precipitate was obtained in the form of a fine powder.
The (PI)BF_4 powder was made into a pellet under the pressure of 98.06 MPa, resulting in a disk-shaped pellet with a diameter of 12mm and a thickness of 1.7mm. Electrical conductivity for the (PI)BF_4 pellet was measured by the four-probe technique at a temperature range of -150 - 25°C.
For conductivity measurements, a quartz probe was placed in a temperature-controlled chamber, and the temperature of the sample in the specimen basket of the probe was measured by using a digital thermometer (Seoul Control Co., SR-6200, G-116) connected to a ceramic thermocouple.

The low temperature was measured using liquid nitrogen. The current and potential through the sample were measured with a digital electrometer (Keithley-616) and a digital multimeter (Keithley-642), respectively.
The conductivities for $(PI)BF_4$ pellets were calculated from the measurements of current and potential at every temperature with a heating rate of 1^oC/min.

Results and Discussions

Electrochemical Analysis

In order to define the electropolymerization mechanisms of aromatic compound-based conductive polymers produced by electrooxidations, a determination of kinetic parameters related to this electrooxidation, besides spectroscopic analysis, should be performed.
The typical equation between currents and the corresponding potentials in the case of an irreversible reaction can be written as the Nernst equation, **[39]**

$$E = E_{l/2} + (RT/\alpha nF)\, \ln[(I_l - I)/I] \qquad (1.1)$$

where n is the number of electrons transferred in the electrode reaction, I_l is the limiting current in a polarographic wave, α is the transfer coefficient, and $E_{l/2}$ is the half-wave potential. That is, the electrochemical parameters of $E_{1/2}$, α, and n can be obtained from a plot of potential vs. $\ln[(I_l-I)/I]$.
In cyclic voltammetry, we considered that peak current (I_p,) and peak potential (E_p,) were related to the scan rates of swept potential (υ).
As for a relationship between the peak current and scan rate, the current must be computed from a baseline of charging current (I_c,) induced by the continuously changing potentials.
Then, the Faradaic current is proportional to the square of the scan rate, and the charging current is also proportional to the scan rate. As for the relationship between peak potential and scan rate, the peak potential is not dependent on the scan rate in the case of a reversible reaction.
On the other hand, peak potential changes with the scan rate in an irreversible system. This fact is important in determining whether or not an electrode system is reversible. There is a method to check for system reversibility simply. In reversible systems, the peak potential width (ΔEp) of anodic and cathodic peak potentials (E_{pa} and E_{pc}) reaches 58/n (mV) at 25^oC.
Figure 7.1 shows a cyclic voltammogram of an [acetonitrile/water/ benzonitrile] solution containing 0.2 M indole monomers and 0.1M $(TEA)BF_4$ as a supporting electrolyte in the potential ranges from -500 to 500 mV at 25^oC. The anodic and cathodic peak potentials are not affected by the change in scan rate. We found this reaction is reversible.
Figure 7.1 shows that the values of E_{pa} and E_{pc} are 320 and 220 mV, respectively, at a scan rate of 100 mV/s. So, the peak potential width (ΔEp) is 120 mV. From the results, we suggest this reaction is reversible, and the number of electrons (n) transferred in this electrode reaction is 2.

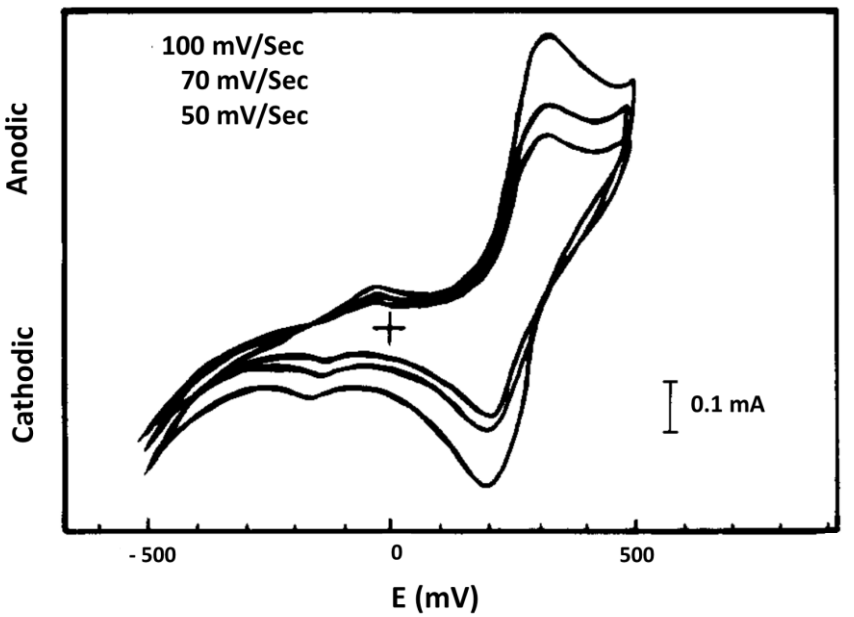

FIGURE 7.1
Cyclic voltammogram of polyindole tetrafluoroborate on a Pt electrode in an [acetonitrile/benzonitrile/water] solution at 25 ^{o}C. [15]

SEM Analysis

In order to analyze the morphology of the (PI)BF_4, polymer coated on the anode, a sample was obtained in an [acetonitrile/benzonitrile/water] solution containing 0.2M indole and 0.1M (TEA)BF_4.
The result of the morphology analysis of the (PI)BF_4 polymer is shown in Figure 7.2. As shown in the scanning electron microscopy (SEM) images, (Figure 7.2), the surface of (PI)BF_4 polymer resembles a growth of aggregates shaped as blossoms.
Also, irregular granules are densely crowded on the polymer. The scattered parts shaped as blossoms are regarded as dopants, and good conductivity is predicted from this compact structure.

TGA Measurements

Thermogravimetric analysis (TGA) for (PI)BF_4 powders shows useful information regarding its thermal stability and physical property.
TGA measurements were performed in a temperature range of 25-800^{o}C under nitrogen. The reaction rate for thermal decomposition, R(*dW/dt*), was calculated by a computer connected to a thermal analyzer.
For a comparison of thermal characteristics of (PI)BF_4 polymers and that of other polyindole-, polyindole hexafluoro-phosphate, (PI)PF_6, and the polyindole perchlorate (PIP) sample was also obtained from the solution with indole monomers, tetraethylammonium hexafluoro-phosphate, (TEA)PF_6, or tetraethyl-ammonium perchlorate (TEAP), respectively.
For a comparison between the reaction rates (R) of polyindole- and polyaniline-polymers doped with the same electrolytes, (PA)BF_4, $PAPF_6$, and PAP, the final result is shown in Figure 7.3. **[16]**

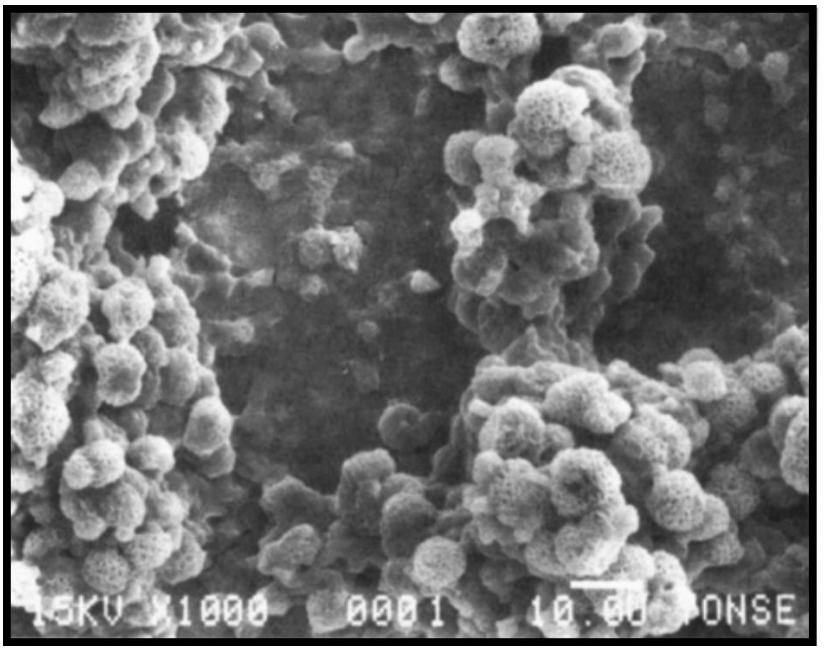

FIGURE 7.2
Scanning electron micrograph (SEM) of a polyindole tetrafluoroborate. [15]

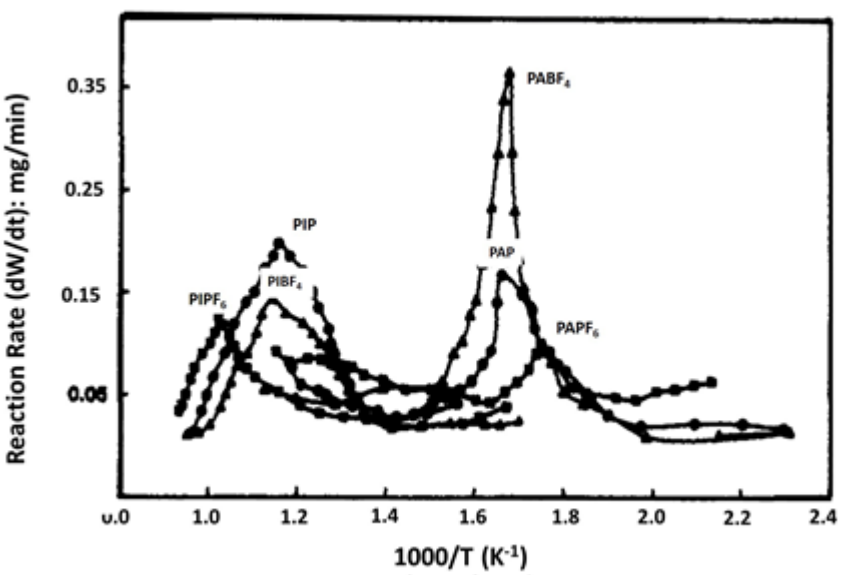

FIGURE 7.3
Temperature dependencies of the reaction rates for various polyaniline and polyindole based-conducting polymers. [15, 16]

Figure 7.3 also shows maximum peaks of the reaction rate (R_{max}) for polyindole- or polyaniline-based polymers. The R_{max} values of (PI)BF_4, $PIPF_6$, PIP, (PA)BF_4, $PAPF_6$, and PAP samples were 0.143 (at 601°C), 0.126 (at 702°C), 0.198 (at 591°C), 0.366 (at 324°C), 0.092 (at 300°C), and 0.166 (at 327°C) mg/min, respectively.

On the basis of these results, the thermal characteristics for polyindole- and polyaniline-based conducting polymers can be explained as follows.

First, the bulk of polyindole systems thermally decomposed at a higher temperature than polyaniline-based polymers. The thermal stability of polyindole systems was greater than that of polyaniline polymers. Polyindole can be utilized in industrial applications requiring higher thermal stability.

Second, the R_{max} values of polyindole-based systems were not seriously affected by the kind of dopant anion. On the other hand, the values of polyaniline polymers were mainly affected by dopant anions. These distinguishable thermal characteristics can be used in various applications because the conductivities of polyindole polymers are similar to those of polyaniline ones.

Conductivity Measurements

Most conductive polymers have the characteristics of a semiconductor in which conductivity increases with temperature.

Conductivities of these amorphous polymers are affected by many factors such as the structure of polymer chains, degree of crystallinity, temperature, pressure, shape, kinds, and amounts of dopants, morphology, density, thickness, potential, and solvent conditions.

Therefore, a determination of possible conduction mechanisms for conductive polymers should be considered carefully.

Scientists have performed experiments on various conduction mechanisms for these amorphous materials, leading to possible conduction models and related equations. **[40-44]**

For example, Mott **[40]** suggested that a related equation based on "hopping conduction" in amorphous semiconductors had a form of $\exp(-T^{-1/4})$. Mott's suggestion was based on the fundamental assumption that the concentration of charge carriers was not affected by the temperature. Mott's equation applies only in temperature ranges of 60-300K. Sheng **[41]** also reported that an equation based on the hopping conduction in sputtered granular metal films had a form of $\exp(-T^{-1/2})$.

Greaves **[42]** reported the following equation for variable range hopping conduction.

$$\sigma T^{1/2} = \exp(-T^{-1/4}) \qquad (1.2)$$

Matare **[43]** reported that electronic conductions which include the grain boundary potential (E_a) are given in the following equation: where A is a constant related to the electric field strength and effective mass of electrons and E_a is the height of the potential barrier.

$$\sigma = AT^{1/2} \exp(-E_a/kT) \qquad (1.3)$$

Zeller **[44]** gave the equation for the "tunneling conduction mechanism."

$$\sigma = \sigma_o \exp(-T^{-1/2}) \qquad (1.4)$$

Electrical conductivity for the pressed pellet of $(PI)BF_4$ was measured by a four-probe method in a temperature range from -150 to 25°C under a low applied field to ensure Ohmic behavior.
Figure 7.4 shows the results of temperature dependence on conductivity. As shown in Figure 7.4, conductivities for the pressed pellet of $(PI)BF_4$ polymers increase linearly with the temperature, satisfying the Arrhenius equation, $\sigma = \sigma_o \exp(-Ea/kT)$. **[45]**

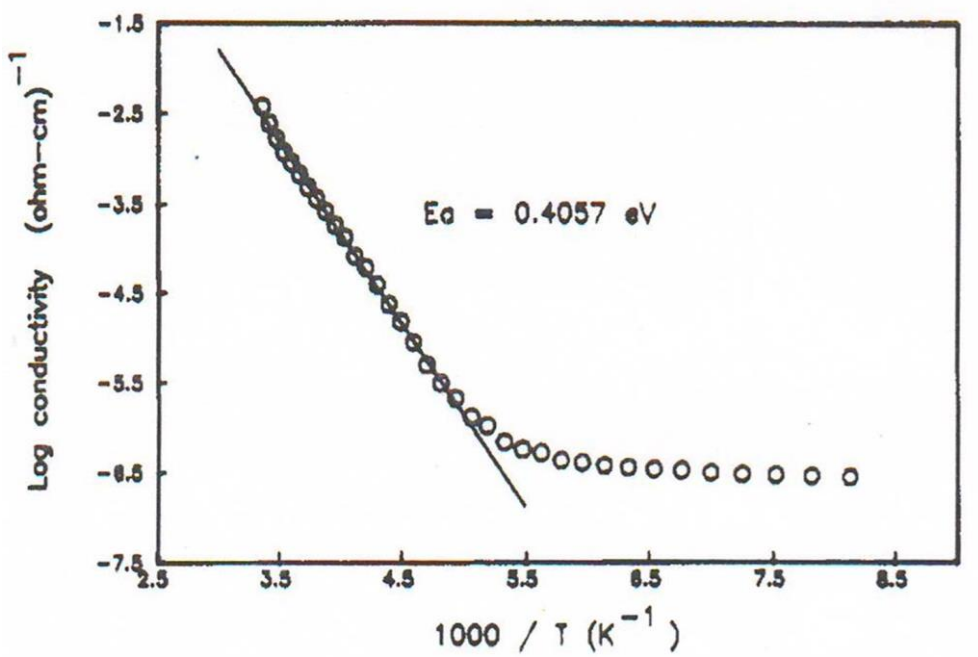

FIGURE 7.4
Electrical conductivity as a function of temperature for a polyindole tetrafluoroborate. [15]

The values of E_a obtained from the slope of the plot and log σ at 25°C were 0.4057 eV and -2.43 S/cm, respectively.
Conductivity measurements changing in relation to the temperature resulted in the plots of the temperature dependence of electrical conductivity based on those equations. **(1-2)-(1-4)**
Among these plots, the one based on equation **(1-2)** for hopping conduction shows better linearity than that based on equations **(1-3)** and **(1-4).** For this reason, we concluded that the possible conduction mechanism of the $(PI)BF_4$ polymer is "a hopping conduction."
The plot based on hopping conduction is shown in Figure 7.5. The conductivity results predict that the polarons act as charge carriers that had formed in the polyindole doped with BF_4^- ions and act as an electron acceptor hopping from state to state.

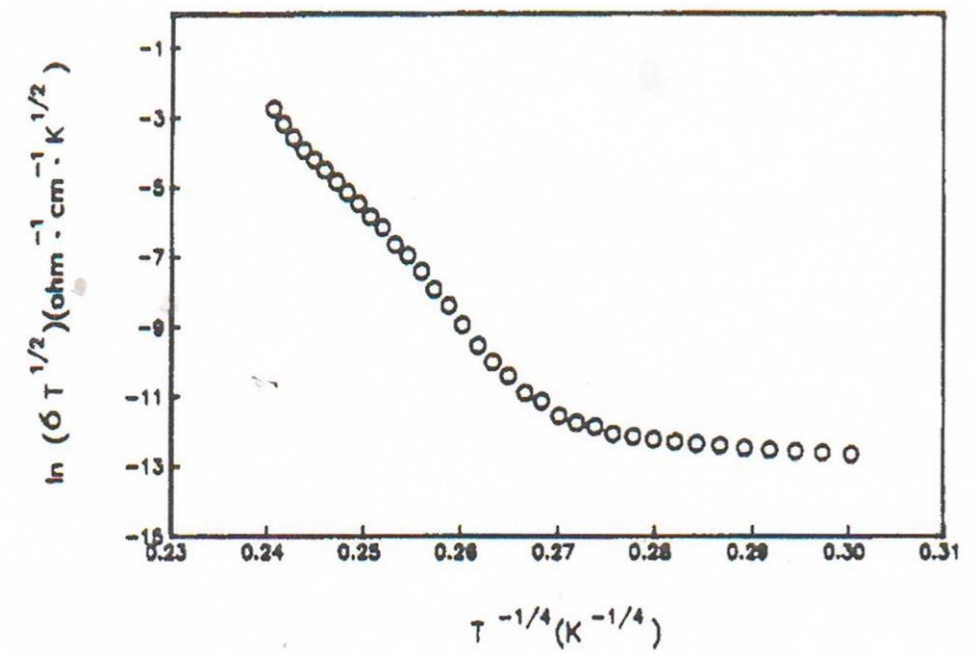

FIGURE 7.5
Temperature dependence of electrical conductivity for a polyindole tetrafluoroborate based on the hopping conduction. [15]

Conduction Mechanism

(PI)BF_4 conducting polymers were obtained from a 0.2M indole monomer in an [acetonitrile/ benzonitrile/water] solution containing 0.1M tetraethylammonium tetrafluoroborate, (TEA)BF_4, as a supporting electrolyte. Electrochemical measurements of the solution concluded that electrooxidation of indole is a reversible reaction, and the number of related electrons was 2. Structural analysis of anodic precipitates suggests that polymerization of indole was based on the formation of radical cations as intermediates.

For a comparison of thermal characteristics of (PI)BF_4 polymers and that of other polyindole-, polyindole hexafluoro-phosphate (PI)PF_6 and polyindole perchlorate (PIP) based samples were also prepared from solutions containing indole, tetraethyl-ammonium hexafluoro-phosphate, (TEA)PF_6, and tetraethylammonium perchlorate (TEAP), respectively. Thermal analyses of polyindole- and polyaniline-based systems were also performed at 25-800°C.

TGA results indicated that most polyindole-based polymers were mainly decomposed at higher temperatures than those of the polyaniline-based systems. Also, maximum values of the reaction rate of thermal decomposition (R_{max}) for the polyindole-based system were not seriously affected by the kind of dopants.

On the other hand, the R_{max} values of the polyaniline-based ones depended on the kind of electron acceptor.

The electrical conductivity of conducting polymer [(PI)BF_4] was measured in the temperature range from -150 to 25°C. The values of E_a obtained from the slope of the plot and log σ at 25°C were 0.4057 eV and -2.43 S/cm, respectively.
Results of conductivity measurements suggested that conduction mechanisms and charge carriers of the conducting polymer [(PI)BF_4] were "hopping conduction" and "polarons," respectively, which then caused BF_4^- anions to act as an electron acceptor.

Molecular Imprinting Synthesis

In this chapter, we introduce "molecular imprinting technology," which is a synthetic process that creates "molecular recognition sites" to detect target molecules. These molecular recognition sites are "receptors or binding sites" that can detect specific molecules. This chapter introduces a sensing polymer, "molecularly imprinting polymer (MIP)," to demonstrate molecular imprinting synthesis.
MIP is a sensing polymer with a specific molecular recognition capability based on "molecular recognition sites" in a highly cross-linked network. These recognition sites can detect an optimal molecularly imprinted polymer formulation for a targeted analyte.
MIPs are used to fabricate chemical sensors or detection devices for detecting target molecules based on the molecular recognition sites. **[28, 46-51]**
Recognition or catalytic sites in MIPs networks are created in cross-linked polymers to react with a template or an imprint molecule. These receptors or binding sites are complementary in size, shape, and functional group reacts to the target molecule, templates. Its morphology and chemical microenvironment of the receptors or binding sites are critical to the sensing or detecting performances.
The imprinting process influences the selectivity and capacity of MIP's networks. In our earlier report **[52],** useful descriptions regarding the MIP's selectivity have been published;
1) Complementary interactions between a template and a functional monomer are necessary to create short-range molecular organization at the receptor site. These interactions include hydrogen bonding, electrostatic, and/or van der Waals forces.
2) The stoichiometry and concentration of a template and monomers influence both polymer morphology and MIP selectivity.
3) The solvent used in the polymerization process, known as the 'porogen,' plays a dual role.
In addition to mediating the interactions between the functional groups and the template molecules, the porogen determines the timing of the phase separation during polymerization [53], which is an important determinant of polymer morphology, porosity, and ultimately accessibility of the binding site. The temperature of polymerization influences the timing of phase separation. Also, the temperature dependence of the equilibrium between the functional monomers and templates affects MIP selectivity and capacity.
The use of MIPs for screening libraries of small molecules has been investigated to fabricate biochemical sensors or detection devices or environmental catalytic sensing devices. **[46-51]**
Figure 7.6 illustrates a molecular imprinting process. As shown in Figure 7.6, the imprinting process involves the polymerization of functionalized monomers in the presence of a template.
Synthesis of molecular receptor sites is a key aspect of the creation of high affinity in molecular recognition.
First, a functional monomer with molecular binding sites reacts with a template and produces a prepolymerized complex. Subsequently, the complex is copolymerized with excess cross-linking

monomers to produce imprinted polymers, which are highly cross-linked (>50%) macroporous thermosets. Porogen was then used to extract templates and to create "receptor or binding sites" in networks. Molecular recognition will take place by rebinding the template molecule to the imprinted receptor site.

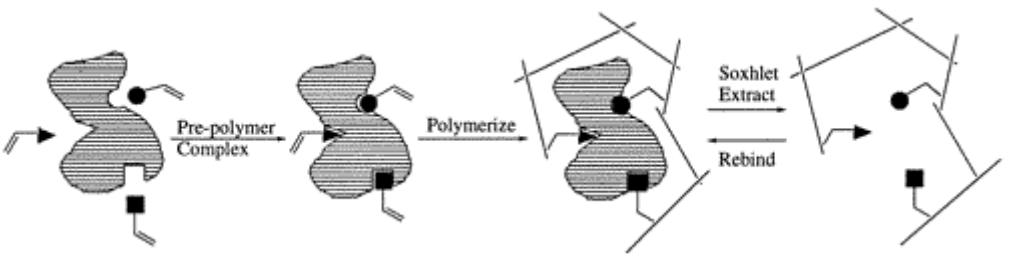

FIGURE 7.6
Schematic diagram of molecular imprinting synthesis of receptor sites.

In molecular imprinting synthesis, highly selective functional polymers with desired templates or target molecules can be imprinted by either the noncovalent **[54]** or covalent **[55]** method.
The non-covalent imprinting process employs a self-assembly strategy in which templates and functionalized monomers pre-assemble by hydrogen bonds, electrostatic and/or van der Waals' forces. (Figure 7.6) This pre-polymer complex is then copolymerized with a cross-linking monomer to provide a network polymer.
Subsequently, the template is removed by extraction with solvent leaving behind the complementary binding site. Templates and receptor molecules are non-covalently linked to each other. For this reason, template molecules can be easily washed away then rebound to imprinted receptor sites to take place in a molecular recognition task.
In contrast, the covalent imprinting process involves the synthesis of a template covalently linked to a polymerizable monomer through a relatively labile bond. Copolymerization with crosslinking monomers produces a polymeric network. The template is then extracted by chemical cleavage, leaving behind highly ordered binding sites.

MIP'S Microfabrication

Recently, as the demand for the development of micro- or nano-scale electronic devices increases, interest in functional polymers integrated on small chips is increasing.
The use of a sensing polymer (MIP) as a molecular recognition element in miniaturized bio- or chemical devices provides an incentive research opportunity to fabricate diagnostic biosensors or drug delivery systems with specific molecular recognition.
MIP's system is a robust thermoset, which tolerates high temperature and harsh environment, but there are challenges in MIP's microfabrication to fabricate smaller and more compact sensor or detection devices at the nano- or micro-scales.
We also introduce "microfabrication technology" which has attracted great attention as part of nanotechnology to integrate small-sized patterns on substrates by high fidelity pattern transfers. This technology has been studied to fabricate nano- or micro-sized electronic devices on a small chip by integrating small patterns of functional materials.
We considered a MIP's system as a good candidate for nano- or micro-sized electronic sensors or detection devices due to the capability of micropatternability on a chip as well as wide applications,

for example, in sensing technology **[48,49],** chromatography **[46,69],** enzymatic catalysis **[57],** and solid-phase extraction. **[47, 58, 59]**
However, the practical applications of MIP are limited due to the low sensitivity and selectivity.
To overcome the limitations in commercialization, untraditional synthesis to produce "high fidelity binding sites" in MIP's systems have been studied. The high-fidelity sites, however, comprise a subpopulation of a broad distribution of sites with a big portion of low selectivity. Such a small amount of high-affinity sites also limits to achieve high sensitivity in MIPs.
In order to take the molecular imprinting technology to the commercial level, "Monoclonal" MIP's particles with high-fidelity recognition sites have been significantly considered; the synthesis, processing, fabrication, separation, and evaluation of "Monoclonal" MIPs system.
The challenge is that each MIP's particle at the nano-scale contains a relatively small number of binding sites and is of a mass, which gives us a high chance for an affinity separation to produce "Monoclonal" MIP's particles with high-affinity sites only. **[46]**

MIP'S Micro-Stereo Lithography

For MIP's system to play an important role in applications of high-performance sensors or diagnostic devices at the nanoscales, we will need MIPs in two- or three-dimensional patterns.
To integrate micropatterned, imprintable MIPs features, we studied technologies, such as soft lithography **[60-62]** or micro-stereo lithography (μSL). **[63]** In this chapter, we demonstrated a two- or three-dimensional microfabrication of MIPs patterns on a glass published in our earlier study. **[64]**
In μSL technology, a directed UV laser beam is focused to 1-2 μm onto the surface of a glass substrate coated with a monomer solution, resulting in localized photopolymerization; synchronized motion of the substrate in the x-y plane is then used to fabricate the pattern of the lowest two-dimensional slice. **[65-67]**
Translation along the z-axis allows the next layer to be written on top of the first layer. Repetition of the photopolymerization results in the third-dimensional micropattern with a layer-by-layer fashion. The fact that polymerization takes place on the desired micro-scale in the x-y plane results from the tight focus of the lithographic lasers used for μSL.
To achieve spatial resolution in the third dimension, however, the photopolymer must have a high enough absorbance at the excitation wavelength to control the depth that the light penetrates into the micropatterns, which in turn determines the height, or "curing depth" of each of the photocured layers.
To create three-dimensional microstructures of the sensing polymer, we used adenine recognition in well-defined, micron-sized MIP's structures, a system was chosen for the biological significance of synthetic receptors capable of nucleotide recognition as shown in our earlier study. **[46]**
In our experiments, the desired selectivity was achieved using 9-ethyl adenine (9-EA) as an imprint molecule and methacrylic acid (MMA) as a functional monomer. A fluorescent derivative, 9-dansyl adenine (9-DA), was also molecularly designed and synthesized for the rebinding study.
The photopolymerizable MIPs monomer mixture contained benzoin ethyl ether (BEE) as a photoinitiator due to the favorable overlap between its absorption maximum and the laser excitation wavelength of the μSL set-up and also contained trimethylolpropane trimethacrylate (TRIM) as a cross-linker. Tinuvin was used as a UV absorber due to its high molar absorption coefficient (151,600 $mol^{-1}cm^{-1}$) at 364 nm to achieve low curing depths. **[64]**

Usually, the evaluation of rebinding selectivity of imprinted polymers employs HPLC analysis. However, the theoretical number of binding sites in the micropatterned polymer generated by μSL technology is below the detection limits for HPLC analysis.
An alternative is to utilize the emission of a fluorescently-tagged analyte to evaluate the binding sites created during the imprinting process. A microstructure that has a higher capacity to rebind an analyte will have a higher fluorescent intensity.
To obtain a fluorescence assay based on our MIP's system based on methacrylic acid/adenine polymer/template, adenine was derivatized at the 9-position using dansyl chloride, yielding a fluorescent 9-dansyl adenine (9-DA). **[68]**
These recognition sites allow a fair degree of freedom in substitution at the 9-position while maintaining overall adenine specificity by the MIPs. It is assumed that the size of the dansyl group will not appreciably affect the rebinding of 9-DA. The rebinding process was then monitored by the total emission intensity from spatial integration over the entire image of each element plotted as a function of time of exposure to the 9-DA analyte solution.
Using the MIPs mixture, we worked on microfabrication of the sensing polymer by μSL technology.
In the fluorescent study, the uptake of 9-DA was greater than in the control without templates and saturated within 25 mins. Also, we found tinuvin didn't affect the affinity or the imprinting process.
The details of the MIP's three-dimensional pattern are as follows.
First, μSL of two-dimensional microstructure was experimentally designed and carried out to determine whether the MIPs micropatterns still had the same selectivity to the bulk polymers.

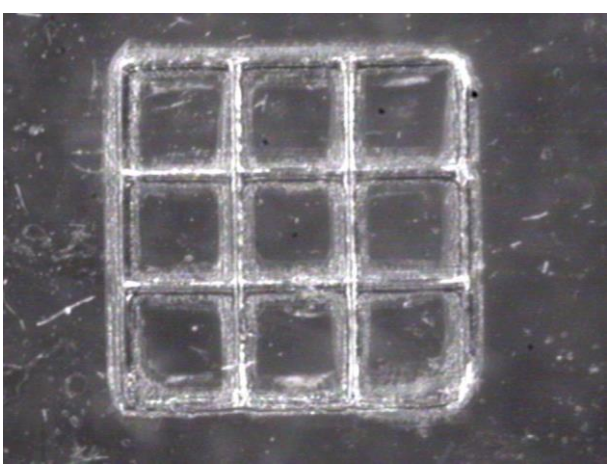

FIGURE 7.7
SEM image of a two-dimensional MIP's imprinted microstructure (600 μm x 600 μm) fabricated by μSL. **[64]**

For this purpose, a MIP's monomer mixture was prepared by containing chloroform (6.271g), TRIM (6.274g), MMA (0.327g), tinuvin (0.013g), BEE (0.131g), and 9-EA (0.050g). A control solution was also prepared without the template. Two-dimensional grids were fabricated from the UV curable MIP monomer solution and a control solution using the 364 nm of the Ar^+ laser and an x-y-z motorized stage.
Figure 7.7 shows an SEM image of the resulting MIPs two-dimensional pattern with a dimension of 600μm x 600μm; the width of the lines comprising the grid was approximately 20 μm.

The microfeatures were washed in isopropyl alcohol then chloroform. Uptake studies were carried out by bathing both solutions in 9-DA chloroform solution ($1.8x10^{-4}$ M) and analyzing the total fluorescence from each sample as a function of time. The two-dimensional MIPs pattern showed a 5:1 preference for 9-DA over the control solution. After the success of two-dimensional microfabrication, we then conducted to generate the three-dimensional MIPs microstructure by building up multiple two-dimensional layers.
Figure 7.8 shows SEM images of the three-dimensional imprinted micropatterns with a height of 100 μm in different magnifications.

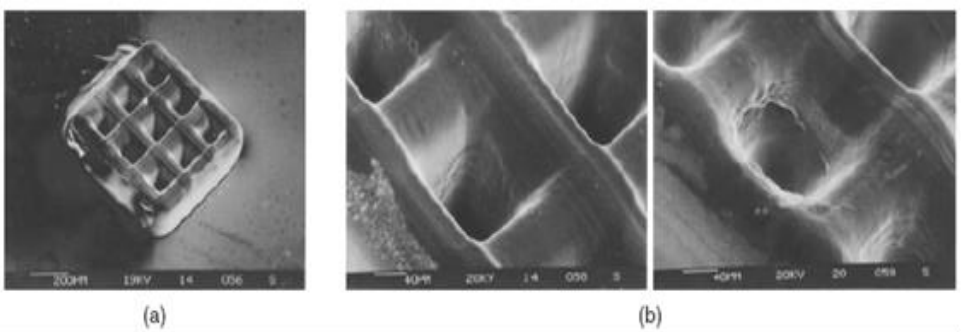

FIGURE 7.8
SEM images of a three-dimensional imprinted microstructure (600 μm x 600 μm x 100 μm) fabricated by μSL. **[64]**

Subsequently, a rebinding study was also performed. The three-dimensional pattern was rinsed and bathed in chloroform for 12 h to wash the 9-EA template. It was then exposed to a solution of 9-DA ($1.08\ x10^{-4}$ M in chloroform) for increasing time intervals, rinsed to remove any residual 9-DA. Rebinding isotherm, fluorescent intensity as a function of exposure time to a $1.08\ x10^{-4}$ M solution of 9-DA in chloroform for both imprinted polymer and control, was plotted.
In the rebinding study, a significantly diminished fluorescent intensity was observed from the blank control compared to the MIP imprinting microfeatures. It indicated that the three-dimensional micropattern of MIP's system is sensitive in molecular recognition tasks.
In short, we concluded that the experimental conditions in the study didn't disrupt the binding interactions between the functional monomers and the template.
We successfully demonstrated the ability to fabricate microsized MIP detection devices based on the three-dimensional features printed on glass through the μSL technology.

Molecular-Level Hybridizations

Molecular-level hybridization is a novel synthetic strategy, that can produce molecular-level composites by hybridization of multiple components at the nano-scales. These nanoscale composites exhibit relatively little phase separation due to molecular-level homogeneity and often produce desired NEW properties.
In general, physically mixed composites on a bulk scale will eventually phase separate. Moreover, composites mixed at the bulk scales retain the original properties of their individual components.
In contrast, nanocomposites mixed at the nano-scales create new properties that individual components do not.

Molecular-level hybridization offers us specific advantages that can't be achieved with the conventional bulk mixing technique. [22, 30] These advantages from molecular-level hybridization are as follows;

1) Hybrid materials prepared by molecular-level hybridization are stiffer, robust materials and result in less phase separations due to the molecular-level homogeneity of multiple phases mixed at the nano-scales.

2) Hybrid materials mixed at the nano-scales often create new properties that individual components do not. We can also design new molecular structures, such as molecular alignments, to produce desired properties.

3) It is used to control the materials' morphology or to modify molecular structures at the nano-scales.

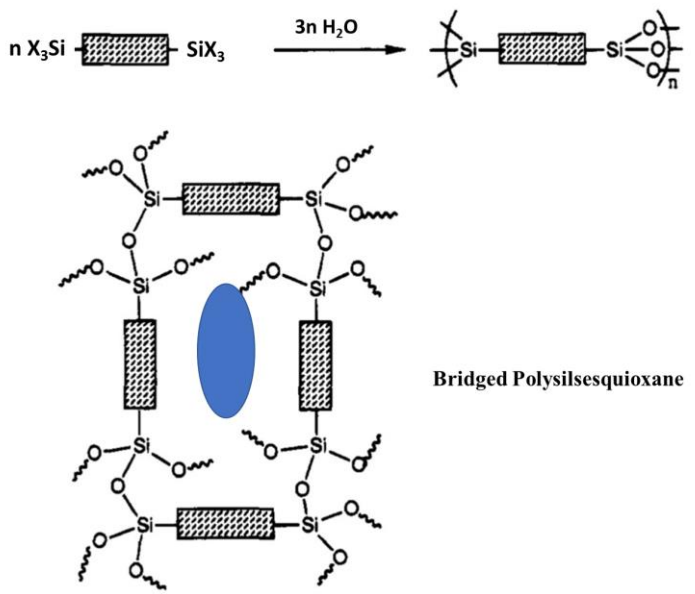

FIGURE 7.9
Bridged polysilsesquixnae designed by the molecular-level hybridization that inserts organic functionality between inorganic oxides in a silicate glass structure. **[18, 21, 22]**

To demonstrate the molecular-level hybridization, an organic/inorganic hybrid glass based on polysilsesquioxane is introduced in this chapter. (Figure 7.9) Polysilsesquoxanes are a family of organically modified hybrid silica that has been widely investigated to develop novel optical devices. The structures of hybrid silicate glass are molecularly designed by the insertion of functional organic spacers between two inorganic networks as shown in Figure 7.9.

Minimized Phase Separation

Hybrid materials can range from physical mixtures of inorganics and organics to nanocomposites that utilize formal chemical linkages between the organic and inorganic domains at the molecular scales.

Hybrid composites from the molecular-level hybridization often show less phase separations which are microscopically homogeneous with uniform distribution of the spacers due to the molecular-level mixing technology at the nanoscales.

To determine the molecular-level homogeneity, we conducted experiments with hybrid silica, "polysilsquioxanes," an organic/inorganic hybrid silica doped with Er^{3+} ions/CdSe nanoparticles.

Recently, rare-earth ions, such as Er^{3+} ions doped into glasses have been widely investigated for optical amplifications. **[4–9]**

However, rare-earth cations doped into normal silica tend to aggregate and end up with a phase separation due to the absence of non-bridging oxygens in the silicate structure. These ion clusters can also result in decreased lasing efficiency in optical applications. In order to achieve a high gain optical amplifier, rare-earth cations must be uniformly doped into the transparent materials.

"Sol-gel synthesis" is an attractive synthetic route to modify the chemical environments of rare-earth ions and also to incorporate a high level of rare-earth ions doped into glassy matrices because of the versatility of the sol-gel monomer mixtures. We devoted our attention to the achievement of chemical homogeneity of Er^{3+} ions doping levels by the molecular-level hybridization to achieve a high homogeneity.

A family of Organic/inorganic hybrid silicate monomers based on polysilsesquioxanes have been molecularly designed by molecular-level hybridization to develop high-performance laser amplifiers. CdSe nanoparticles were also synthesized for further manipulation of the photochemical environment of erbium ions in the matrix in our earlier study. **[27]**

In our work **[27],** the results of mixing efficiency using three different sol-gel monomers for the mixing test T-mixture, H-mixture, and F-mixture systems have been published to determine the phase separations.

In the mixing test, T-mixture refers to a sol-gel monomer solution based on TEOS (tetraethyl orthosilicate), H-mixture refers to a sol-gel solution based on 1,6-bis(triethoxysilyl)hexane, and F-mixture refers to a solution based on octafluoro-1,6-hexanediol bis(3-triethoxysilyl)propyl carbamate. Among the sol-gel monomer mixtures, H- and F-xerogel systems are organically modified hybrid materials designed by molecular-level hybridization.

During the mixing test, we observed that the TEOS-based mixtures revealed a substantial degree of undesirable phase separations after doping with the Er^{+3} ion sources and CdSe nano-particles while the hybrid sol-gel mixtures revealed relatively less phase separations.

As is evident from erbium-ion incorporation in details, the T- mixture showed a significant phase separation even at the lower erbium concentration. In contrast, those hybrid sol-gel mixtures accommodate and homogeneously distribute the Er^{3+} source without significant phase separations. It is apparent that the TEOS mixture has a rather limited solubility of erbium ions.

Subsequently, we added CdSe nano-particles into the sol-gel mixtures containing the erbium-ions as dopants. The comparative homogeneity of the three silicate mixtures containing both erbium isopropoxide and CdSe nanoparticles is shown in the study. [27]

TEOS-mixture revealed the CdSe nano-particles segregated; the orange-colored CdSe nanoparticles were observed to phase separate within the TEOS-mixture. In a hybrid system of H-mixture, the CdSe nano-particles mixed better than the T-xerogel one; most of the CdSe particles were dissolved except some of the undissolved orange-colored CdSe residues toward the middle of the container. In a fluorinated mixture, CdSe nanoparticles were incorporated without any phase separation.

This result indicated that the hybrid sol-gel systems molecularly mixed by the molecular-level hybridization have the capability of uniformly incorporating both types of dopants without significant phase separations.

Creation of New Properties

The molecular-level hybridization offers us specific advantages, including the creation of new properties that were not found in the original components by the insertion of functional spacers between networks to "rearrange" the designed molecular structure at the nano-scales.

In our earlier study, the creation of new property arising from molecular level hybridization has been demonstrated using hexylene-bridged polysilsesquioxane doped with Cr^0/CrO_x nanophases; the resulting hybrid composite showed a new optical property, "effective diffraction grating," that individual components do not. **[29]**

Usually, when light passes through a solid, it generates linear waves due to rigid solid lattice frames. Surprisingly, the organic/inorganic hybrid composite doped with Cr^0/CrO_x nanophases generates a huge "acoustic response" as much as a liquid.

To identify the nanoalignment designed in the hexylene-bridged structure, a high-resolution transmission electron microscopic (HRTEM) analysis was performed; TEM images revealed an unusual nanofringe pattern, which rose from the lattice fringes of the aligned alkyl-spacers in the silicate matrix. The morphology of the hybrid silica showed substantial regions of dark contrast, highly organized nano-periodic structures in TEM images. **[29]**

We believed that the novel nano-periodic structures observed from the hybrid composite were sustained over substantial domains and appear to arise from organically modified glassy lattice fringes.

Electron diffraction analysis of these dark regions shown in the TEM images was also carried out. In electron diffraction pattern, it revealed the circled diffraction patterns arise from crystalline Cr metal and a set of diffractions near the center of the beam corresponding to the nanofringe structures observed in TEM images.

From the diffraction pattern corresponded to the nano-fringes, a lattice space of the nano-striped patterns observed in TEM images was calculated about 50 Å from a distance between two diffraction spots in two sets of diffraction patterns.

We suggested that the novel molecular design of arranging alkylene-spacers between inorganic networks at the nano-scales resulted in "a molecular level grating characteristic" when the laser light passes by those periodic carbon chains.

In laser experiments, the coefficient of phonon diffraction of the Cr-doped hybrid glass which is proportional to the coefficient of thermal conductivity was FIVE times smaller than that of normal glass; in other words, the thermal conductivity of the Cr-doped hybrid glass was FIVE times less than normal glass. The diffraction efficiency, the absorption light efficiency of the hybrid glass (45%), was higher than methanol (25%); which means, the compressibility of the hybrid glass was as effective as the liquid.

The acoustic response generated from the hybrid glass was as compressive as liquid thus the acoustic refractive intensity generated from the hybrid sol-gel glass was as strong as a liquid. Therefore, the heat gets transferred into expansion or compression waves (acoustic waves) effectively in the hybrid glass. The hybrid glass serves as a heat generator or heat energy storage material.

From this result, we suggest that the Cr^o-doped hybrid glass can be used for various optical applications including diffraction beam modulators.

As demonstrated in our study, the effective optical grating at the molecular scales was a new phenomenon that hitherto hasn't been discovered. In other words, the new property, which did not exist in the original components, was created by the molecular-level mixing process.

Control of Morphology or Molecular Structures

Scientists are looking for new synthetic methods to control the morphology and have discovered that one goal and advantage of molecular level hybridization is controlling the morphology of materials. Despite the rather complex origins of porosity, the possibility of "engineering" porosity was considered by assembling nano or micro-sized molecular building blocks into a three-dimensional scaffolding. [30, 68] It was investigated from a challenge that the gaps in such a scaffolding might be controlled by the size of the building blocks.

In this chapter, we demonstrated porosity control through molecular-level hybridization. Due to the ability to dope nanoparticles into optically transparent glasses without cracking issues, highly nanoporous organic/inorganic hybrid glasses have been used to control the hybrid's morphology during molecular-level hybridization.

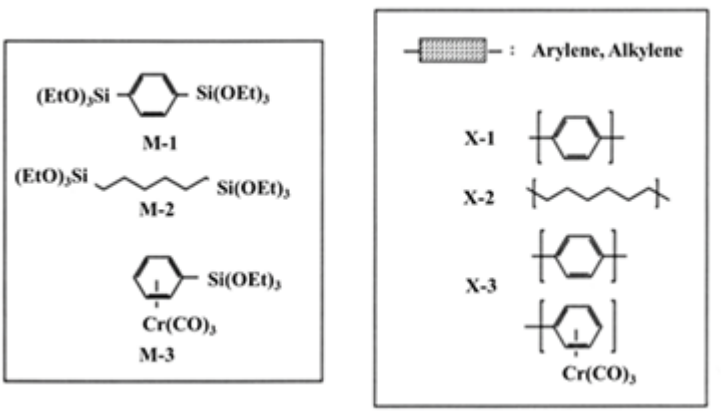

FIGURE 7.10
The molecular-level hybridization: xerogels (X-1, 2, 3) prepared by inserting different sol-gel processable organic spacers (M-1, 2, 3). **[18]**

The hybrid glass used in this study was bridged polysilsesquioxanes, designed by the molecular-level hybridization as "molecular composite" of inorganic oxides and organic polymers. (Figure 7.9)

The family of bridged polysilsesquioxanes provides a range of materials with "engineered" microporosity. **[30]** It showed extremely high surface areas with narrow pore distributions confined to a range of 100 Å or lower. **[18, 30, 68-70]**

In molecular-level hybridization, the average pore size can be controlled by the choice of molecular building block and by processing conditions. **[18]** As shown in Figure 7.10, microporous polyphenylene silsesquioxane (X-1) xerogel was prepared from 1,4-bis(triethoxysilyl)benzene monomer (M-1). The X-2 xerogels are also prepared from 1,6-bis(triethoxysilyl)hexane monomer (M-2). M-3 was molecularly designed as Cr sources to dope the nanoparticles into a hybrid silicate matrix. **[18, 20, 21]**

These porous xerogels can serve as a confinement matrix for the controlled growth of nano-sized particles. The average size of the semiconductor particle may be determined by the choice of polysilsesquioxane confinement matrix as illustrated in Figure 7.10.

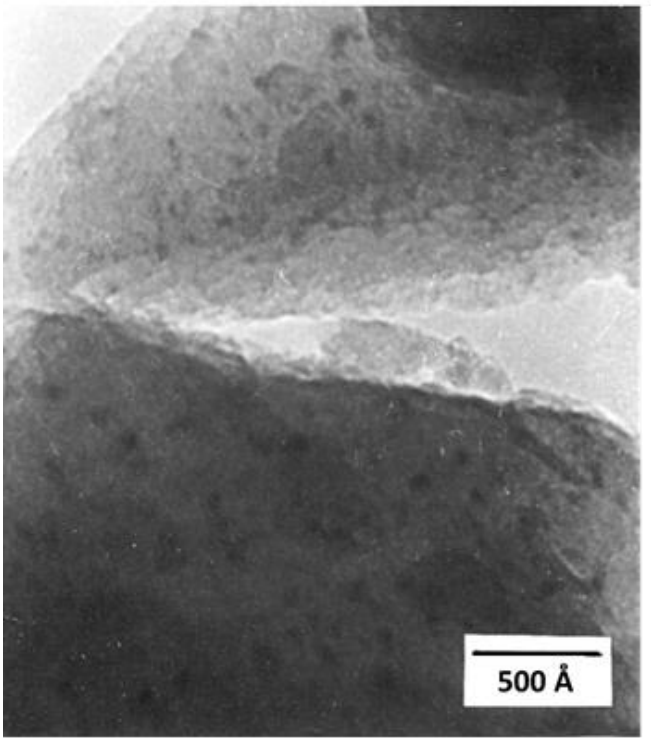

FIGURE 7.11
HRTEM image of a xerogel, X-1, doped with CdS. The dark spots (average diameter 58 Å) are microcrystalline CdS particles. **[18]**

A sol-gel processable monomer (M-1) used in our doping experiments had a BET surface area of 531 m^2/g and a relatively narrow distribution of pores with an average diameter of 34Å (BJH theory). **[18, 69, 71]** Using the xerogel (X-1), the CdS doping process was carried out on dried xerogels (100-250 μm particle size) by first soaking for two days in 0.05 M $CdCl_2$ (ethanol/water-1:4), filtering and washing with water followed by treatment with a 0.1M solution of Na_2S.
A pale-yellow color appeared immediately. The material was filtered, washed with water, then dried (vacuum oven, 24 h, 25°C).
Figure 7.11 shows an HRTEM image of a xerogel, X-1, doped with CdS nanoparticles. The dark spots are microcrystalline CdS with an average diameter of 58 Å. Subsequently, utilization of this flexibility was also demonstrated by the growth of CdS particles in a hexamethylene bridged polysilsesquioxane (X-2), a material prepared by sol-gel process of 1,6-bis (triethoxysilyl)hexane (M-2). **[18]**

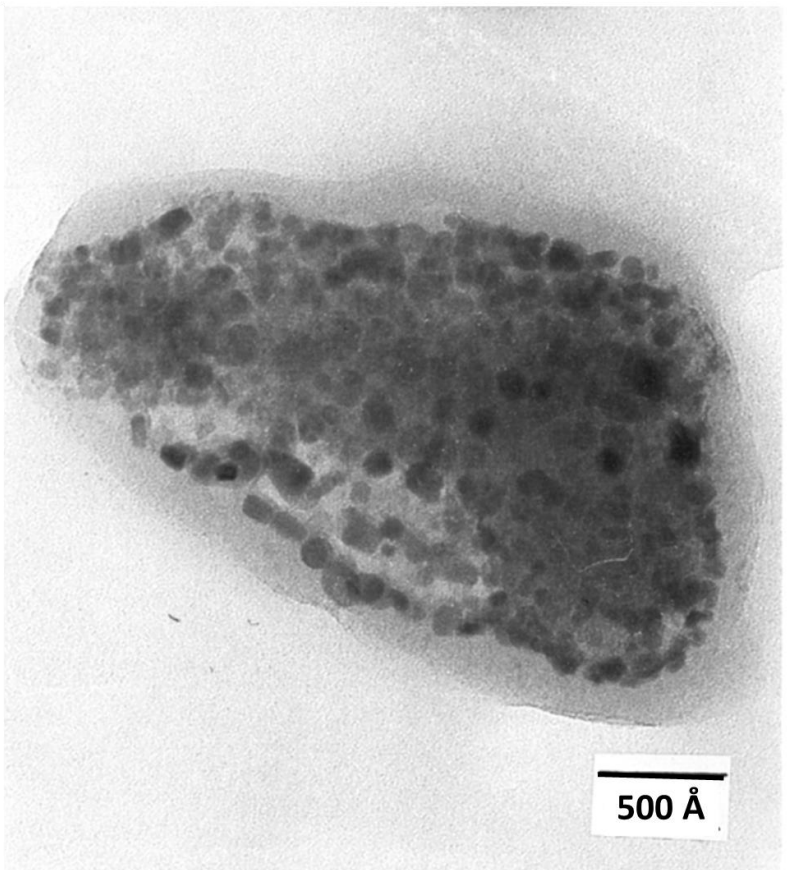

FIGURE 7.12
HRTEM image of a CdS doped xerogel, X-2.
The dark spots (average diameter 90Å) are microcrystalline CdS particles. [**18]**

This dried xerogel has a BET surface area of 533 m^2/g with an average pore diameter of 43 Å. Utilizing doping techniques identical to those of the previous example, microcrystalline CdS particles were produced with an average particle diameter of 90±16Å as measured directly from TEM images and from analysis of the shift in the UV hand edge. (Figure 7.12)
The identity of the CdS spots observed in the TEM images was confirmed in X-2 by EDAX and the electron diffraction pattern.
A demonstration of this approach also includes a xerogel sample doped with chromium clusters using a sol-gel processable chromium precursor (M-1 and M-3) shown in Figure 7.10. A doped xerogel (X-3) was prepared from chromium tricarbonyl monomer (M-3) and 1,4-bis(triethoxysilyl)benzene (M-1) (2:98 % by wt.).
TEM image of the doped xerogel, X-3, (Figure 7.13) revealed the appearance of irregularly shaped dark features that ranged in size from 25 to 100 Å. Focusing on these new dark features, the EDAX and the electron diffraction pattern confirmed their elemental composition and microcrystallinity of the chromium clusters.

The particle shape and other features of internally doped porous materials may reveal structural information of the internal porosity. In short, these demonstrate a molecular-scaled synthesis of "internal doping" and matrix confinement of the developing metal or semiconductor clusters within a microporous hybrid material, polysilsesquioxane xerogels.
It demonstrates that the material's porosity can be controlled by the molecular-level hybridization and also microporous polysilsesquioxanes can be used as a confinement matrix for the growth of nano-sized semiconductor particles and that the morphology of the individual xerogel "controls" the size of the resulting nano-sized particle.

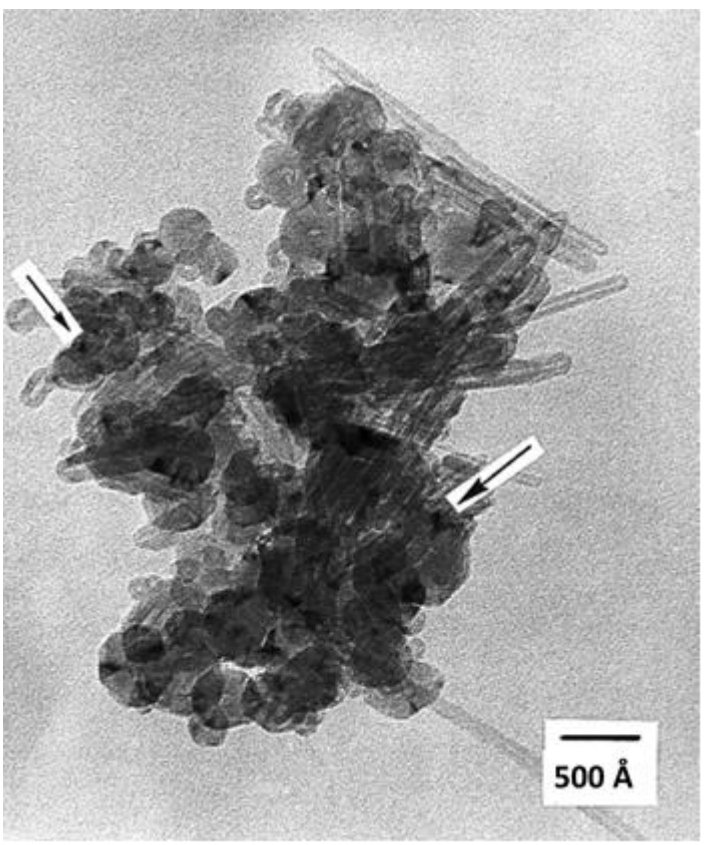

FIGURE 7.13
HRTEM image of a Cr-doped xerogel, X-3. The dark spot irregular regions of approximate dimensions 25-100 Å (see arrows), are microcrystalline Cr particles. **[18]**

Conclusions

Nanotechnology is based on the integration of all disciplines of science, including physics, chemistry, biology, materials science, and engineering

The author has a multidisciplinary background in applied physics, synthetic chemistry, materials science, and nanotechnology which enables the creation of desired properties in advanced functional materials to develop optoelectronic devices for physics and engineering applications.
This chapter introduces how chemists can discover novel synthetic routes and contribute to leading nanotechnology when the challenge to discover novel syntheses of functional nanomaterials needs to be reconciled at the nanoscale level.
New synthetic approaches to advanced functional materials include;

1) An electrochemical synthesis method to produce conductive polymers is introduced. Polyindole tetrafluoroborate, (PI)BF_4, was electrochemically polymerized using cyclic voltammetry from a 0.2 M indole in an [acetonitrile/benzonitrile/water] solution containing 0.1 M tetraethyl-ammonium tetrafluoroborate as a supporting electrolyte.
The (PI)BF_4 powder was obtained as insoluble precipitates using a potential of 0.7 V on the anode. The electrochemical measurements of this solution concluded that the electrooxidation of indole was a reversible reaction, and the number of related electrons is 2.
From conductivity measurements, we concluded that the possible conduction mechanism of the (PI)BF_4 polymer was "hopping conduction." The conductivity measurements also predicted that the polarons acted as charge carriers that had formed in the polyindole doped with BF_4^- ions and acted as an electron acceptor hopping from state to state.

2) "Molecular imprinting synthesis" was introduced to produce functional polymers. Molecularly imprinted polymer (MIP) was introduced as a sensing polymer that has "molecular recognition sites (receptors or binding sites)" which detect specific target molecules for detection purposes and so MIP can be used to detect specific target molecules by fabrication of detection/sensing devices or environmental catalytic interests.
Binding sites are created by "molecular imprinting synthesis." It begins with a copolymerization of crosslinking monomers and functional monomers in the presence of the template. The template is then removed which leaves the recognition sites in the polymer network. Molecular recognition will take place by the extraction/rebinding process of templates to detect specific target molecules. MIP will have the capability of selectively re-binding the template to the binding sites.
MIPs are also micropatternable material printed through μsL technology that fabricates two- or three-dimensional microfeatures capable of recognizing target analytes. The patterns were imprinted on glass without disrupting the binding interactions between the functional monomers and the template.

3) Molecular-level hybridization is a molecular-level mixing technique that mixes up components at the nanoscales. The resulting composites have shown unique advantages that can't be achieved from conventional composites mixed at the bulk scales.
First, molecular-level hybrid composites prepared by molecular-level hybridization are stiffer, robust materials and showed less phase separations due to the molecular-level homogeneity.
Secondly, molecular-level hybrid composites are capable of the creation of new, desired properties that individual components do not.
Third, it allows us to control materials' morphology or molecular structure at the nano-levels.
As demonstrated, chemists contribute to nanotechnology to meet our needs for advanced materials by the discovery of novel synthetic approaches to drive nanotechnology forward to the next level.

This chapter introduces new syntheses that will be the shortcuts leading to breakthroughs to have a significant impact on nanotechnology.

References

1. Brus, L. E., Electron-electron and electron-hole interaction in small semiconductor crystallites-the size dependence of the lowest excited electron state, *J. Chem. Phys.,* 80, pp. 4403-4409, **1984.**
2. Bawendi, M. G., Steigerwald, M. L. and Brus, L. E., The quantum mechanics of larger semiconductor clusters ("quantum dots"), *Annu. Rev. Phys. Chem.,* 41, pp. 477-496, **1990.**
3. Alivisatos, A. P., Perspectives on the physical chemistry of semiconductor nanocrystals, *J. Phys. Chem.*, 100, pp. 13226-13239, **1996.**
4. Krätschmer, W., Lamb, L. D., Fostiropoulos, K. and Huffman, D. R. M., Solid C_{60}: a new form of carbon, *Nature,* 347(6291), pp. 354-358, **1990.**
5. Mintmire, J. W., Dunlap, B. I. and White, C. T., Are fullerene tubules metallic?, *Phys. Rev. Lett.,* 68 (5), pp. 631-634, **1992.**
6. Huynh, W. U., Peng, X. G. and Alivisatos, A. P., CdSe nanocrystal rods/poly(3-hexylthiophene) composite photovoltaic devices, *Adv. Mater.,* 11 (11), pp. 923-927, **1999.**
7. Bruchez, M., Moronne, M., Gin, P., Weiss, S. and Alivisatos, A. P., Semiconductor nanocrystals as fluorescent biological labels, *Science,* 281 (5385), pp. 2013-2016, **1998.**
8. Norris, D. J., Sacra, A., Murray, C. B. and Bawendi, M. G., Measurement of the size-dependent hole spectrum in CdSe quantum dots, *Phys. Rev. Lett.,* 72, pp. 2612-2615, **1994.**
9. Murray, C. B., Kagan, C. R. and Bawendi, M. G., Synthesis and characterization of monodisperse nanocrystals and close-packed nanocrystal assemblies, *Annual Review of Materials,* 30, pp. 545-610, **2000.**
10. O'Brien, S., Brus, L. E. and Murray, C. B., Synthesis of monodisperse nanoparticles of barium titanate: toward a generalized strategy of oxide nanoparticle synthesis, *J. Am. Chem. Soc.,* 123(48), pp. 12085-12086, **2001.**
11. Choi, K. M., Kim, K. H. and Choi, J. S., Electrical conductivity of the system ThO_2- Er_2O_3, *J. Phys. Chem. Solids,* 49(9), pp. 1027-1034, **1998.**
12. Choi, K. M., Kim, K. H. and Choi, J. S., The chemical and physical properties of electrochemically prepared polyaniline p-toluenesulfonates, *J. Phys. Chem.,* 93, pp. 4659-4664, **1989.**
13. Kim, D., Choi, K. M., Kim, K. H. and Choi, J. S., Electrical conductivity of the solid solutions XTm_2O_3 + (1-X)ThO_2; 0.01<X<0.15, *J. Phys. Chem. Solids,* 50(8), pp. 821-828, **1989.**
14. Park, J. S., Choi, K. M., Kim, K. H. and Choi, J. S., Electrical conductivity of the solid solutions $XThO_2$ + (1-X) Ho_2O_3; 0.02<X<0.10, *J. Phys. Chem. Solids,* 50(9), pp. 909-913, **1989.**
15. Choi, K. M., Kim, C. Y. and Kim, K. H., Polymerization mechanism and physicochemical properties of electrochemically prepared polyindole tetrafluoroborate ($PIBF_4$), *J. Phys. Chem.,* 96 (9), pp. 3782-3788, **1992.**
16. Choi, K. M. and Kim, K. H., The chemical and physical properties of electrochemically prepared polyaniline hexafluorophosphate ($PAPF_6$), *J. Appl. Poly. Sci.,* 44(5), pp. 751-763, **1992.**

17. Choi, K. M., Jang, J. H. and Kim, K. H., The chemical and physical properties of electrochemically prepared polyindole hexafluorophosphate ($PIPF_6$), *Mol. Cryst. Liq. Cryst.,* 220, pp. 201-205, **1992.**
18. Choi, K. M. and Shea, K. J., New materials for the synthesis of quantum-sized semiconductor and transition-metal particles. Microporous polysilsesquioxanes as a confinement matrix for particle growth. *Chem. Mater.,* 5, pp. 1067-1069, **1993.**
19. Choi, K. M. and Shea, K. J., Amorphous polysilsesquioxanes as a confinement matrix for quantum-sized particle growth. Size analysis and quantum size effect of CdS particles grown in porous polysilsesquioxanes, *J. Phys. Chem.,* 98, pp. 3207- 3214, **1994.**
20. Choi, K. M. and Shea, K. J., Preparations of nano-sized chromium clusters and chromium clusters coated with CdS phases in the sol-gel matrix by internal doping method, *J. Am. Chem. Soc.,* 116, pp. 9052-9060, **1994.**
21. Choi, K. M., Hemminger, J. C. and Shea, K. J., New procedure for preparation of colloidal CdS and heterogeneous Cr/CdS phases in sol-gel matrices: pore structure analysis and characterization, J. *Phys. Chem.,* 99 (13), pp. 4720-4732, **1995.**
22. Choi, K. M. and Shea, K. J. **(1998)** Hybrid materials for electrical and optical applications, sol-gel synthesis of bridged polysilsesquioxanes, Photonic Polymer Systems, Fundamentals, Methods, and Applications edited by D.L. Wise et al., World Scientific Publishing Co. Pte. Ltd., 49, Chapter 12.
23. Dickenns, S. H., Stansbury, J. W., Choi, K. M. and Floyd, C. J. E., Photopolymerization kinetics of methacrylate dental resins, *Macromolecules,* 36, pp. 6043-6053, **2003.**
24. Choi, K. M. and Rogers, J. A., A photocurable poly(dimethylsiloxane) chemistry designed for soft lithographic molding and printing in the nanometer regime, *J. Am. Chem. Soc.,* 125, pp. 4060-4061, **2003.**
25. Choi, K. M., Advanced soft lithography at the nano-scale regime; new photocurable silicone elastomers with adjustable physical toughness, *J. Phys. Chem. B,* 109, pp. 21525-21531, **2005.**
26. Hung, L. H., Choi, K. M., Tseng, W. Y., Tan, Y. C., Shea, K. J. and Lee, A. P., The generation of CdS nanoparticles by dynamic droplet fusion; comparison of CdS nanoparticles prepared by direct/microfluidic mixing, *Lab on a chip,* 6, pp. 174-178, **2006.**
27. Choi, K. M., A chemical approach to improve photoluminescence environments of erbium-ions/CdSe nanoparticles doped into organic/inorganic hybrid glasses for laser amplifier material applications, *Mater. Chem. Phys.,* 103, pp. 176-182, **2007.**
28. Choi, K. M., Microfluidic approach for the synthesis of micro- or nano-sized molecularly imprinted polymer particles, *Research Letters in Materials Science*, pp. 458158-458160, **2008.**
29. Choi, K. M. and Shea K. J., Optical glass effectively generating a large acoustic wave for diffraction beam modulator applications, *J. Phys. Chem. C,* 112 (46), pp. 18173-18177, **2008.**
30. Choi, K. M. **(2012).** Novel optical device materials-molecular-level hybridization, Optical devices in communication and computation edited by Peng Xi, Intech publisher: Open science/Open minds, Chapter 10.
31. Nakata, M., Taga, M. and Kise, H., Synthesis of electrical conductive polypyrrole films by interphase oxidative polymerization effects of polymerization temperature and oxidizing agent, *Polymer Journal-Nature,* 24(5), pp. 437-441, **1992.**
32. Ateh, D. D., Navsaria, H. A. and Vadgama, P., Polypyrrole-based conducting polymers and interactions with biological tissues, *J. R. Soc. Interface*, 3(11), pp. 741-752, **2006.**

33. Kinyanjui, J. M., Wijeratne, N. R., Hanks, J. and Hatchett, D. W., Chemical and electrochemical synthesis of polyaniline/platinum composites, *Electrochimica Acta,* 51 (14), pp. 2825-2835, **2006.**
34. Latonen, R.-M., Esteban, B. M., Kvarnström, C. and Ivaska, A., Electrochemical polymerization and characterization of a poly(azulene)-TiO_2 nanoparticle composite film, *J. Apply. Electrochem.,* 39(5), pp. 653-661, **2009.**
35. Macit, H., Sen, S. and Sacak, M., Electrochemical synthesis and characterization of polycarbazole, *J. Apply. Poly. Sci.,* 96(5), 894-898, **2005.**
36. Tüken, T., Yazıcı, B. and Erbil, M., Electrochemical synthesis of polythiophene on nickel-coated mild steel and corrosion performance, *Apply. Surface Sci.,* 239(3-4), pp. 398-409, **2005.**
37. Waltman, R. J., Bargon, J. and Diaz, A., Electrochemical studies of some conducting polythiophene films, *J. Phys. Chem*. 87(8), pp. 1459-1463, **1983.**
38. Tourillon, G. and Garnier, F., New electrochemically generated organic conducting polymers, *J. Electroanal. Chem. Interfacial Electrochem.,* 135(1), pp. 173-178, **1982.**
39. Wahl, D., A short history of electrochemistry. *Galvanotechtnik,* 96(8), pp. 1820-1828, **2005.**
40. Mott, N. F., Conduction in non-crystalline materials, *Philos. Mag.,* 19(160), pp. 835-852, **1969.**
41. Sheng, P., Abeles, B. and Ark, Y., Hopping conductivity in granular metals, *Phys. Rev. Lett.,* 31(1), pp. 44-47, 1973.
42. Greaves, G. N., Small polaron conduction in V_2O_5/P_2O_5 glasses, *J. Non-Cryst. Solids,* 11(5), pp. 427-446, **1973.**
43. Matare, H. F., Carrier transport at grain boundaries in semiconductors, *J. Appl. Phys.,* 56, pp. 2605-2631, **1984.**
44. Zeller, H. R., Electrical conductivity of one-dimensional conductors, *Phys. Rev. Lett.,* 28(22), pp. 1452-1455, **1972.**
45. Arrhenius, S.A., Über die Dissociationswärme und den Einfluß der Temperatur auf den Dissociationsgrad der Elektrolyte, *Z. Phys. Chem.,* 4, pp. 96-116, **1889.**
46. a) Spivak, D., Gilmore, M. A. and Shea, K. J., Evaluation of binding and origins of specificity of 9-ethyladenine imprinted polymers, *J. Am. Chem. Soc.,* 119 (19), pp. 4388–4393, **1997.** B) Shea, K. J., Spivak, D. A. and Sellergren, B., Polymer complements to nucleotide bases. Selective binding of adenine derivatives to imprinted polymers, *J. Am. Chem. Soc.,* 115(8), pp. 3368-3369, **1993.**
47. Masqueè, N., Marceè, R. M. and Borrull, F., Molecularly imprinted polymers: new tailor-made materials for selective solid-phase extraction, *Trends Anal. Chem.,* 20 (9), pp. 477-486, **2001.**
48. Kriz, D., Ramstrom, O. and Mosbach, K., Molecular imprinting – new possibilities for sensor technology, *Anal. Chem.,* 69, pp. A345-A349, **1997.**
49. Haupt, K. and Mosbach, K., Molecularly imprinted polymers and their use in biomimetic sensors, *Chem. Rev.,* 100, pp. 2495-2504, **2000.**
50. Piletsky, S. A., Karim, K., Piletska, E. V., Day, C. J., Freebairn, K. W., Legge, C., Turner, A. P. F., Recognition of ephedrine enantiomers by molecularly imprinted polymers designed using a computational approach, *Analyst,* 126, pp. 1826-1830, **2001.**
51. Dirion, B., Lanza, F., Sellergren, B., Chassaing, C., Venn, R. and Berggren, C., Selective solid-phase extraction of a drug lead compound using molecularly imprinted polymers prepared by the target analog approach, *Chromatographia,* 56, pp. 237-241, **2002.**

52. Batra, D. and Shea, K. J., Combinatorial methods in molecular imprinting, *Curr. Opin. Chem. Bio.,* 7, pp. 434-442, **2003.**
53. Guyot, A. and Bartholin, M., Design, and properties of polymers as materials for fine chemistry, *Prog. Polym. Sci.,* 8, pp. 277-331, **1982.**
54. Mosbach, K., Molecular imprinting, *Trends in Biochemical Sciences,* 19, pp. 9-14, **1994.**
55. Shea, K. J., Molecular imprinting of synthetic network polymers: the de novo synthesis of macromolecular binding and catalytic sites, *Trends Polym. Sci.,* 2, pp. 166-173, **1994.**
56. Ansell, R. J., Kriz, D. and Mosbach, K., Molecularly imprinted polymers for bioanalysis: Chromatography, binding assays and biomimetic sensors, *Curr. Opin. Biotechnol.,* 7, pp. 89-94, **1996.**
57. Wulff, G., Enzyme-like catalysis by molecularly imprinted polymers, *Chem. Rev.,* 102, pp. 1-27, **2002.**
58. Lanza, F. and Sellergren, B., The application of molecular imprinting technology to solid-phase extraction, *Chromatographia,* 53, pp. 599-611, **2001.**
59. Masque, N., Marce, R. M. and Borrull, F., Molecularly imprinted polymers: New tailor-made materials for selective solid-phase extraction, *Trands Anal. Chem*, 20, pp. 477-486, **2001.**
60. Yan, M. and Kapua, A., Fabrication of molecularly imprinted polymer microstructures, *Anal. Chim. Acta.,* 435(1), pp. 163-167, **2001.**
61. Whitesides, G. M., Ostuni, E., Takayama, S., Jiang, X. and Ingber, D. E., Soft lithography in biology and biochemistry, *Annu. Rev. Biomed. Eng.,* 3, pp. 335-373, **2001.**
62. Vozzi, G., Flaim, C. J., Bianchi, F., Ahluwalia, A. and Bhatia, S., Microfabricated PLGA scaffolds: A comparative study for application to tissue engineering, *Mater. Sci. Eng. C,* 20(1-2), pp. 43-47, **2002.**
63. Witzgall, G., Vrijen, R., Yablonovitch, E., Doan, V. and Schwartz, B. J., Single-shot, two-photon exposure of commercial photoresist for the production of three-dimensional structures, *Opt. Lett.,* 23(22), pp. 1745-1747, **1998.**
64. Conrad. P. G., Nishimura, P. T., Aherne, D., Schwartz, B. J., Wu, D., Fang, N., Zhang, X., Roberts, M. J. and Shea, K. J., Functional molecularly imprinted polymer microstructures fabrication using microstereolithographic techniques, *Adv. Mater.,* 11, pp. 5274-5285, **2003.**
65. Manias, E., Chen, J., Fang, N. and Zhang, X., Polymeric micromechanical components with tunable stiffness, *Appl. Phys. Lett.,* 79(11), pp. 1700-1702, **2001.**
66. Ikuta, K. and Hirowatari, K., Real three-dimensional microfabrication using stereolithography and metal molding, in MEMS 93, Fort Lauderdale, FL, Proc. *IEEE Micro Electro-Mech. Syst.,* pp. 42-47, **1993.**
67. Jiang, X. N., Sun, C., Zhang, X., Xu, B. and Ye, Y. H., Microstereolithography of lead zirconate titanate thick film on a silicon substrate, *Sensors and Actuators,* 87, pp. 72-77, **2000.**
68. Loy, D. A. and Shea, K. J., Bridged polysilsesquioxanes. Highly porous hybrid organic-inorganic materials, *Chem. Rev.,* 95 (5), pp. 1431-1442, **1995.**
69. Shea, K. J., Loy, D. A, and Webster, O. W., Arylsilsesquioxane gels and related materials. New hybrids of organic and inorganic networks, *J. Am. Chem. Soc.* 114(17), pp. 6700-6710, **1992.**
70. Corriu. R. J. P., Moreau, J. J. E., Thepot, P., and Wang, C. M. M., New mixed organic-inorganic polymers: Hydrolysis and polycondensation of bis(trimethoxysilyl)organometallic precursors, *Chem. Mater.* 4(6), pp. 1217-1224, **1992.**

71. a) Barrett, E. P., Joyner, L. G., Halenda, P. P., The determination of pore volume and area distributions in porous substances. I. Computations from nitrogen isotherms, *J. Am. Cem. Soc.* 73(1), pp. 373-380, **1951.** b) Oscik, J. and Cooper, I. L. **(1982).** In Adsorption; John Wiley & Sons: New York.